INTERNATIONAL JOURNAL FOR NUMERICAL METHODS IN FLUIDS
Int. J. Numer. Meth. Fluids **31**: 801–819 (1999)

APPLICATION OF THE LATTICE-BOLTZMANN METHOD TO STUDY FLOW AND DISPERSION IN CHANNELS WITH AND WITHOUT EXPANSION AND CONTRACTION GEOMETRY

RAJINDER KUMAR[a], SRIRAM S. NIVARTHI[a], H. TED DAVIS[a,*], D.M. KROLL[b] AND ROBERT S. MAIER[b]

[a] *Department of Chemical Engineering and Materials Science, Army High Performance Computing Research Center, University of Minnesota, 421 Washington Avenue SE, Minneapolis, MN 55455, USA*
[b] *Army High Performance Computing Research Center and Minnesota Supercomputer Center Incorporated, 1100 Washington Avenue S, Minneapolis, MN 55415, USA*

SUMMARY

The lattice-Boltzmann (LB) method, derived from lattice gas automata, is a relatively new technique for studying transport problems. The LB method is investigated for its accuracy to study fluid dynamics and dispersion problems. Two problems of relevance to flow and dispersion in porous media are addressed: (i) Poiseuille flow between parallel plates (which is analogous to flow in pore throats in two-dimensional porous networks), and (ii) flow through an expansion–contraction geometry (which is analogous to flow in pore bodies in two-dimensional porous networks). The results obtained from the LB simulations are compared with analytical solutions when available, and with solutions obtained from a finite element code (FIDAP) when analytical results are not available. Excellent agreement is found between the LB results and the analytical/FIDAP solutions in most cases, indicating the utility of the lattice-Boltzmann method for solving fluid dynamics and dispersion problems. Copyright © 1999 John Wiley & Sons, Ltd.

KEY WORDS: lattice-Boltzmann; lattice gas; dispersion; porous media

1. INTRODUCTION

The lattice-Boltzmann (LB) method was first proposed by McNamara and Zanetti [1] and is a relatively new method for solving flow problems. The method was modified by Higuera and Jimenez [2] when they introduced a linearized collision operator. Further generalizations by Chen *et al.* [3] and Qian *et al.* [4] ensure that the equilibrium distribution is isotropic, Galilean invariant and that the pressure is velocity independent. All these models [3–5] use the single relaxation time approximation first introduced by Bhatnager *et al.* [6]. A wide range of problems have been studied using the LB method, including viscous flows [1–4], multiphase flows [7,8], magnetohydrodynamics [9] and chemically reacting flows [10].

The LB technique is purely local and parallel in nature, and is an active research topic because of the huge interest in increasing the speed of computations using parallel architecture. The LB method approaches fluid dynamics from the microscopic kinetic level and may be

* Correspondence to: Office of the Dean, Twin Cities Campus, University of Minnesota, 105 Walter Library, 117 Pleasant Street SE, Minneapolis, MN 55455, USA.

CCC 0271–2091/99/210801–19$17.50

Received 10 February 1998
Revised 20 October 1998

interpreted as a finite difference solution of the discrete velocity Boltzmann equation utilizing a linearized collision operator. In more general terms, the LB method denotes any numerical method that solves a Boltzmann equation for an ensemble-averaged distribution of moving, interacting particles on a lattice. The LB equation describes the evolution of particle populations rather than the motions of individual particles. The evolution is determined so that the Navier–Stokes equation is recovered in a Chapman–Enskog expansion [11].

The LB scheme consists of a particle-streaming step followed by a collision. It results in a simple logic that is easily implemented on parallel computers. The loads on the different nodes in a parallel computer are automatically balanced since approximately the same numbers of operations are carried out at each lattice node.

This paper is interested in the utility and accuracy of the LB method as a potential alternative to other conventional approaches to study fluid flow problems. The focus of this research has been to test the accuracy of the LB method in flow geometry commonly encountered in the study of flow in porous media. With this aim, the LB method has been applied to study two specific problems: (i) Poiseuille flow between two parallel plates, and (ii) flow through an expansion–contraction (or dilation) geometry. In the pore bodies, study of the recirculations are very important because they trap the contaminants, which makes it difficult to clean a porous media. A study of the recirculations in expansion–contraction geometry using the finite element method was carried out by Ruth and Ma [12]. A study of recirculations in the flow using the LB method around an octagonal cylinder was performed by Noble *et al.* [13].

In the present work, the accuracy of the LB method is gauged by comparing the LB results with analytical solutions where available and with results generated by a finite element code called FIDAP (Fluid Dynamics International, Inc.). The LB method has also been used to study transient flow problems. The LB calculations were carried out on the CM-5 Connection Machine.

2. THEORY

The LB method employed in this work uses a nine-speed, square lattice. The nine vectors are (see Figure 1):

$$\mathbf{e}_{0,0} = (0, 0), \tag{1}$$

$$\mathbf{e}_{1,i} = \left(\cos\frac{2\pi(i-1)}{8}, \sin\frac{2\pi(i-1)}{8}\right), \quad i = 1, 2, 3, 4, \tag{2}$$

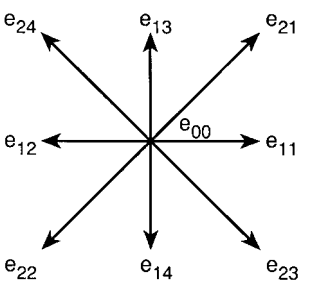

Figure 1. The nine-speed square lattice used in the lattice Boltzmann simulations carried out in this paper. Unit vectors directions in the nine-speed model are shown in the inset.

$$\mathbf{e}_{2,i} = \sqrt{2}\left(\cos\frac{2\pi(i-1)}{8}, \sin\frac{2\pi(i-1)}{8}\right), \quad i = 1, 2, 3, 4. \tag{3}$$

The discretized Boltzmann equation employed has the form

$$f_{\sigma i}(\mathbf{x} + \mathbf{e}_{\sigma i}, t+1) - f_{\sigma i}(\mathbf{x}, t) = \Omega_{\sigma i}, \tag{4}$$

where $f_{\sigma i}$ is the particle distribution function; the subscripts σ and i refer to the type of particle and velocity direction respectively. $\Omega_{\sigma i}$ is the collision operator representing the rate of change of the particle distributions due to collisions, and is given by

$$\Omega_{\sigma i} = -\frac{1}{\tau}\left[f_{\sigma i}(\mathbf{x}, t) - f_{\sigma i}^{\mathrm{eq}}(\mathbf{x}, t)\right], \tag{5}$$

where τ is the single relaxation time that controls the rate of approach to equilibrium and $f_{\sigma i}^{\mathrm{eq}}$ is the equilibrium particle distribution function.

The mean density and velocity of the LB fluid particles are given by

$$\sum_{\sigma}\sum_{i} f_{\sigma i} = \rho, \tag{6}$$

$$\sum_{\sigma}\sum_{i} f_{\sigma i}\mathbf{e}_{\sigma i} = \rho\,\mathbf{u}. \tag{7}$$

The equilibrium particle distribution functions used in this work are

$$f_{00}^{\mathrm{eq}} = \rho\left[\frac{2}{7} - \frac{2}{3c_{\mathrm{s}}^2}(\mathbf{u}\cdot\mathbf{u})\right], \tag{8}$$

$$f_{1,i}^{\mathrm{eq}} = \rho\left[\frac{1}{7} + \frac{1}{3c_{\mathrm{s}}^2}(\mathbf{e}_{1,i}\cdot\mathbf{u}) + \frac{1}{2c_{\mathrm{s}}^4}(\mathbf{e}_{1,i}\cdot\mathbf{u})^2 - \frac{1}{6c_{\mathrm{s}}^2}(\mathbf{u}\cdot\mathbf{u})\right], \quad i = 1, 2, 3, 4, \tag{9}$$

$$f_{2,i}^{\mathrm{eq}} = \rho\left[\frac{1}{28} + \frac{1}{12c_{\mathrm{s}}^2}(\mathbf{e}_{2,i}\cdot\mathbf{u}) + \frac{1}{8c_{\mathrm{s}}^2}(\mathbf{e}_{2,i}\cdot\mathbf{u})^2 - \frac{1}{24c_{\mathrm{s}}^2}(\mathbf{u}\cdot\mathbf{u})\right], \quad i = 1, 2, 3, 4, \tag{10}$$

For the above equilibrium distribution, the velocity of sound is

$$c_{\mathrm{s}} = \sqrt{\frac{3}{7}}. \tag{11}$$

It is interesting to note that the velocity of sound is independent of the compressibility of the LB fluid. This means that a disturbance in the fluid will always move with constant velocity.

In the lattice-Boltzmann method, LB fluid particles with mass distributed in all nine vector directions exist at each site (not to be confused with the particles or mass of the actual fluid). Collisions of LB fluid particles take place at each site followed by the redistribution of mass and momentum along each direction; this is followed by the streaming step. This process is known to recover the Navier–Stokes equation for the solvent and the convection–diffusion equation for the tracer.

In order for a comparison with the real fluids, it is necessary only to match the Reynolds number and geometry in the LB simulations for incompressible flow. The physical velocity and pressure fields can be expressed in terms of dimensionless velocity and pressure in the LB method calculations.

2.1. Recovery of Navier–Stokes equations using the LB method

The incompressible Navier–Stokes equations can be recovered from the LB technique in a Chapman–Enskog expansion in the Knudsen number δ [11]:

$$\partial_t(\rho u_\alpha) + \partial_\beta(\rho u_\alpha u_\beta) = -\partial_\alpha(p) + \delta\partial_\beta(2\nu\rho S_{\alpha\beta}) - \delta\partial_\beta\left(\tau - \frac{1}{2}\right)\partial_\gamma(\rho u_\alpha u_\beta u_\gamma) + O(\delta^2), \tag{12}$$

where

$$S_{\alpha\beta} = \frac{1}{2}(\partial_\alpha u_\beta + \partial_\beta u_\alpha), \quad \alpha, \beta, \gamma = 1, 2, \tag{13}$$

and τ is the relaxation time.

It may be seen that if the last two terms of $O(\delta u^3)$ and $O(\delta^2)$ in Equation (13) are ignored, the following equations are obtained:

$$\partial_t(\rho u_\alpha) + \partial_\beta(\rho u_\alpha u_\beta) = -\partial_\alpha(p) + \delta\partial_\beta(2\nu\rho S_{\alpha\beta}), \quad \alpha, \beta = 1, 2. \tag{14}$$

The kinematic viscosity, ν, for the square lattice is given by

$$\nu = \frac{2\tau - 1}{6}. \tag{15}$$

The incompressible Navier–Stokes equation can be approximated if the velocity of the fluid is much less than the velocity of the sound, thereby making the term $O(\delta u^3)$ negligibly small, and by choosing a finer lattice, which will make the term $O(\delta^2)$ smaller. The presence of the error terms in the above equations produces compressibility effects in the LB fluid, and the amount of compressibility is dependent on the Mach number. Further, it can be seen in Equation (12) that for one-dimensional flows, the term $O(\delta u^3)$ becomes equal to zero.

2.2. Boundary conditions for the flow problem

A major challenge in the accurate application of the LB method has been the implementation of the appropriate boundary conditions. The simple bounce back boundary condition that is directly taken from the lattice gas method is of first-order accuracy in space and time [14–17]. Skordos [18] suggested a boundary condition based on a finite difference scheme which is of second-order accuracy in space and time. This, however, requires the numerical computation of expensive finite differences. Noble *et al.* [19,20] recently proposed a new boundary condition, which is mathematically rigorous and produces results of greater accuracy. In the case of the square lattice, however, these boundary conditions can only be applied on vertical or horizontal walls. They cannot be applied at the corners, where the system becomes either over- or underdetermined.

Note that in the case of bounce back, the wall is located half way between the row/column of nodes adjacent to the wall [16]. However, in the case of the energy boundary condition introduced by Noble *et al.*, the lattice nodes are located exactly on the walls (see Figure 2).

A nine-speed square lattice is used in this work. The fluid is at rest initially, so that the initial distribution functions are set equal to their equilibrium values. In the case of the boundary conditions introduced by Noble *et al.* [19,20], where in general boundary nodes can have zero velocity (at walls) or non-zero velocity (at inlet or at outlet), incoming unknown distributions can be calculated by solving the following set of equations for the three undetermined distributions and the density of the LB fluid particle, ρ:

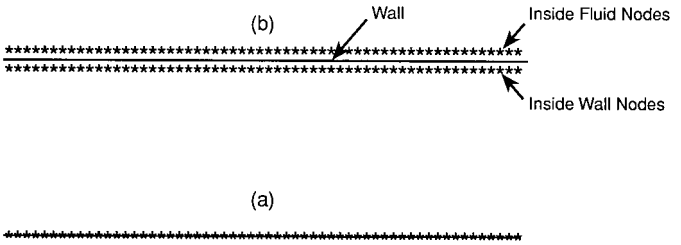

Figure 2. Location of the wall in the case of (a) energy boundary condition introduced by Noble *et al.*, (b) bounce back boundary condition.

$$f_{11}+f_{12}+f_{14}+2f_{21}+2f_{22}+2f_{23}+2f_{24}=2\rho\varepsilon+\rho(V_x^2+V_y^2), \tag{16}$$

$$f_{11}+f_{12}+f_{13}+f_{14}+f_{21}+f_{22}+f_{23}+f_{24}=\rho, \tag{17}$$

$$f_{11}+f_{12}+f_{21}+f_{24}-f_{22}-f_{23}=\rho V_x, \tag{18}$$

$$f_{12}-f_{14}+f_{21}-f_{24}+f_{22}-f_{23}=\rho V_y, \tag{19}$$

$$\varepsilon=c_s^2-\tau c_s^2(\nabla\cdot\mathbf{u})\delta+o(\delta^2). \tag{20}$$

3. RESULTS FOR FLOW

3.1. Results of Poiseuille flow in a channel

The LB method has been used to study Poiseuille flow in a channel by various other authors. For completeness, results for Poiseuille flow using (a) bounce back and (b) energy boundary condition proposed by Noble *et al.* [19,20] are presented. Figure 3 shows the co-ordinates of the various points of the channel on a 41×1000 lattice.

Figure 4(a) and (b) shows the velocity profiles for the bounce back and the energy boundary conditions respectively. The simulation was carried out on a 41×1000 lattice for a Reynolds number of 50. The initial condition for the LB simulation was a liquid of uniform density at rest. A parabolic velocity profile with a maximum velocity of 0.1 at the centerline was imposed at the inlet ($x = 1$) and outlet ($x = 1000$) of the channel. Note that since the walls are located between two lattice rows for bounce back boundary conditions, a lattice width containing 41 nodes in the domain corresponds to a width of 41. In the case of the energy boundary condition, a lattice width containing 41 nodes corresponds to a width of 40. In order to have the same Reynolds number in the two cases, a slightly different value of τ was used in the two simulations.

3.2. Results of flow through a dilation

The LB method has been applied to study flow in the expansion–contraction geometry as a preliminary step to studying the transport of chemical species in the porous media, where recirculations are often present. Figure 3(b) shows the co-ordinates of various points on a 241×1000 lattice of the expansion–contraction geometry.

The initial condition for LB simulation was a liquid of uniform density at rest. A parabolic velocity profile, with a center velocity of 0.1, was then imposed at the entrance ($x = 1$) and at the outlet ($x = 1000$). For the chosen value of τ, this corresponds to a Reynolds number of 50.

Excellent agreement was found between the LB simulation results for the steady state velocity profiles using both the bounce back as well as the energy boundary conditions and the results obtained from FIDAP. A comparison between the LB method and FIDAP results for the x and y components of the velocity at $x = 520$ along the y-axis is shown in Figure 5(a)–(d) (using the bounce back as well as the energy boundary conditions). The flow in a expansion–contraction geometry is characterized by a quasi-parabolic, time-independent velocity profile. Large recirculation vortices develop on either side of the expansion–contraction geometry, as can be seen in Figure 6. These vortices moderate the rate of mass transfer from the walls of the cavity to the channel. Note that the flow velocities in the recirculation region, as shown in Figure 5, are much smaller than the peak channel velocity. This result suggests why increased pumping rates, which would increase the channel velocity, do not necessarily improve the efficiency of pump-and-treat remediation in the porous media.

4. LATTICE–BOLTZMANN METHOD FOR THE STUDY OF THE DISPERSION

An LB scheme for simulating a reaction–diffusion system was introduced by Dawson *et al.* While they used a hexagonal lattice, the following equation is recovered for the reaction–diffusion system for the square lattice (nine-speed model):

$$\frac{\partial n_s}{\partial t} + \nabla\cdot(n_s\mathbf{u}) - c_s^2\left(\tau_s - \frac{1}{2}\right)\nabla^2 n_s = R_s, \tag{21}$$

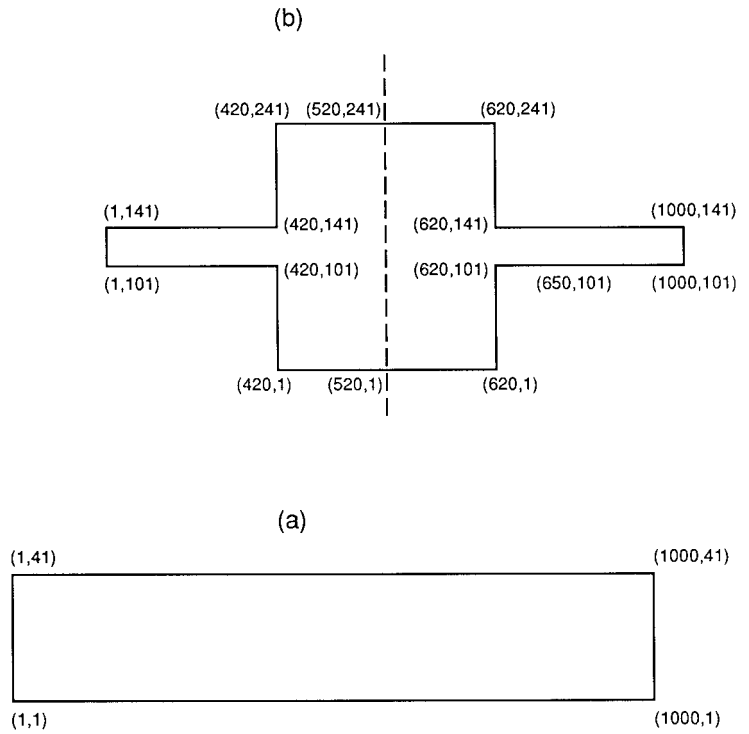

Figure 3. Co-ordinates of various points on a (a) 41×1000 lattice of the channel, and (b) 241×1000 lattice of the expansion–contraction geometry.

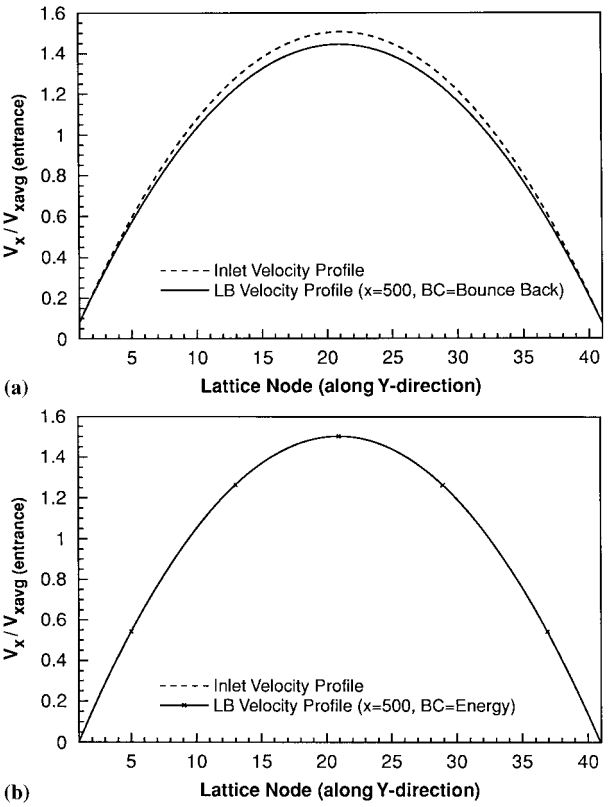

Figure 4. Velocity profiles for Poiseuille flow between two parallel plates with the (a) bounce back boundary condition ($\tau = 0.664$); (b) energy boundary condition ($\tau = 0.66$).

where n_s is the concentration of the species s and R_s is the reaction rate for species s. The diffusivity of species s is given by

$$D_s = c_s^2(t_s - 0.5), \tag{22}$$

where c_s is the velocity of sound and τ_s is the relaxation time for species s.

Dawson *et al.* [10] expressed the equilibrium distribution of the tracer ($f^{eq}_{\sigma i(s)}$) in terms of the equilibrium distribution of the solvent ($f^{eq}_{\sigma i}$) and the ratio of their densities (n_s/n_0) as

$$f^{eq}_{\sigma i(s)} = \frac{n_s}{n_0} f^{eq}_{\sigma i}. \tag{23}$$

4.1. Boundary conditions for the dispersion problem

In the simulation of tracer dispersion, a no-flux boundary condition needs to be applied at the walls. The bounce back condition can approximate zero flux at the walls since the LB particles are reflected back into the flow system.

Dispersion was studied by imposing a step input in the tracer concentration at the inlet and comparing the mean (cup-mixed) concentration at a specified downstream location. The inlet

distributions for the tracer were calculated using the inlet distributions of the main fluid (solvent):

$$f_{\sigma i(\mathrm{s})} = \frac{n_{\mathrm{s}}}{n_0} f_{\sigma i}. \tag{24}$$

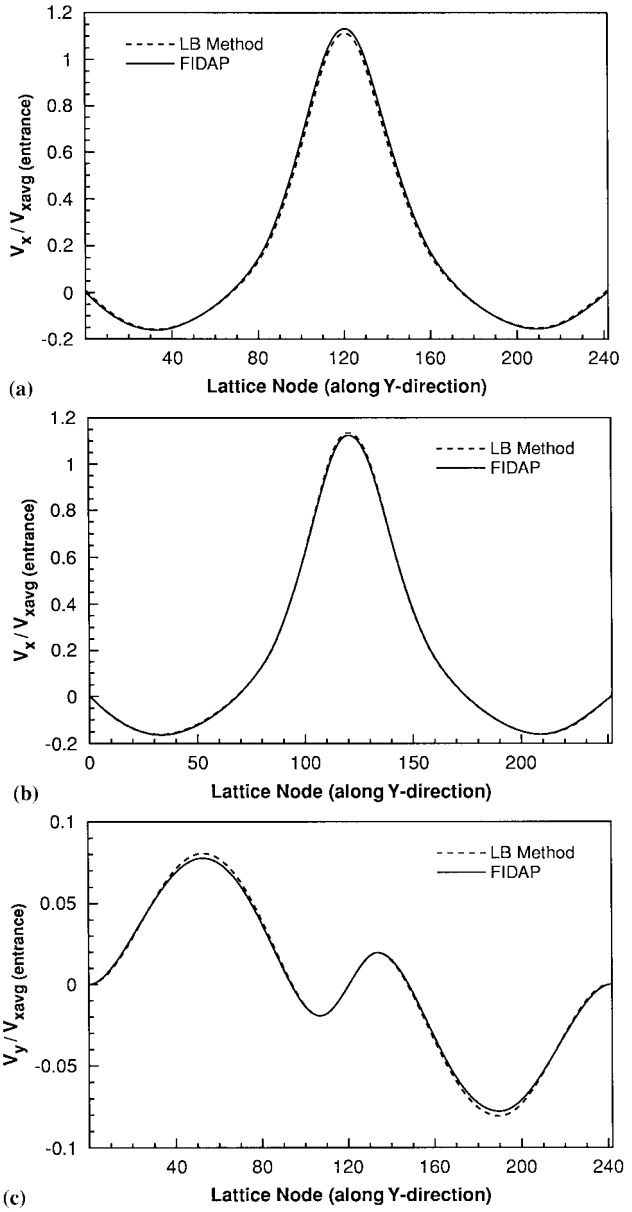

Figure 5. Comparison of the x and y component velocities between the LB method and FIDAP at $x = 520$ and along the y-axis using the bounce back and the energy boundary conditions: (a) x component velocity using bounce back; (b) x component velocity using the energy boundary condition; (c) y component velocity using bounce back; (d) y component velocity using the energy boundary condition.

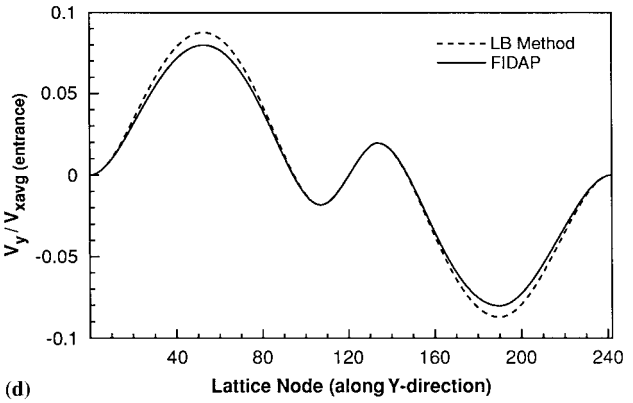

Figure 5 (*Continued*)

4.2. Application of the LB method to study Taylor–Aris dispersion in a channel

Taylor [21] and Aris [22] showed that when $R_s = 0$, Equation (11), in certain conditions reduces to the following convection–dispersion equation:

$$\frac{\partial C_m}{\partial t} + U\frac{\partial C_m}{\partial x} = D\frac{\partial^2 C_m}{\partial x^2}, \tag{25}$$

where U is the average velocity, D is the dispersion coefficient and C_m is the mean concentration at a cross-section of a pipe. They are given by following expressions:

$$D = D_m + \frac{d^2U^2}{48D_m}, \tag{26}$$

$$C_m(x) = \frac{\int_0^{2\pi}\int_0^R C(r,x)r\,\mathrm{d}r\,\mathrm{d}\theta}{\int_0^{2\pi}\int_0^R r\,\mathrm{d}r\,\mathrm{d}\theta}. \tag{27}$$

The above equation can be written in dimensionless form as follows:

$$\frac{\partial C'_m}{\partial t'} + \frac{\partial C'_m}{\partial x'} = \frac{D}{Ud}\frac{\partial^2 C'_m}{\partial x'^2}, \tag{28}$$

where

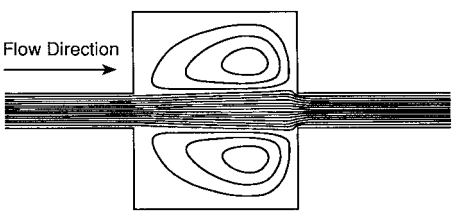

Figure 6. Recirculation vortices on either side of the expansion–contraction geometry.

$$C'_{\mathrm{m}} = C_{\mathrm{m}}/C_{\mathrm{m0}}, \tag{29}$$

$$t' = \frac{t}{(d/U)} \tag{30}$$

and

$$x' = \frac{x}{d}. \tag{31}$$

U is the average velocity. For the flow in a circular pipe, $U = 0.5U_{\max}$.

For flow between two parallel plates separated by height h, $U = (2/3)U_{\max}$, and the coefficient of dispersion is given by [14]:

$$D = D_{\mathrm{m}} + \frac{h^2U^2}{210D_{\mathrm{m}}}. \tag{32}$$

The dimensionless convection–dispersion equation is given by (28) with $d = h$, and dimensionless time and distance are given by (30) and (31) with $d = h$.

There is an analytical solution to Equation (25) for the following initial and boundary conditions:

Initial condition:
$t = 0, \quad C_{\mathrm{m}} = C_{\mathrm{m0}}$ at $x = 0, \quad C_{\mathrm{m}} = 0$ at $x > 0$.

Boundary conditions:
$C_{\mathrm{m}} = C_{\mathrm{m0}}$ at $x = 0$ for all t,
$C_{\mathrm{m}} = 0$ at $x = L$ for all t.

The analytical solution is

$$\frac{C_{\mathrm{m}}}{C_{\mathrm{m0}}} = \frac{1}{2}\exp\left(\frac{xU}{D}\right)\operatorname{erfc}\left(\frac{x+Ut}{2.0\sqrt{Dt}}\right) + \frac{1}{2}\operatorname{erfc}\left(\frac{x-Ut}{2.0\sqrt{Dt}}\right). \tag{33}$$

The dispersion problem has been solved using the LB scheme for the case of Poiseuille flow between two parallel plates. The simulations were performed for the following lattice sizes: 11×1000, 21×1000 and 41×1000. For the solvent, a parabolic velocity profile was imposed at all cross-sections of the channel with a maximum velocity of 0.1 at the center. When the steady state for the solvent was achieved, a step input of the tracer was introduced at the inlet of the channel in accordance with the following equation:

$$f_{\sigma i(\mathrm{s})} = \frac{n_{\mathrm{s}}}{n_0} f_{\sigma i}. \tag{34}$$

Plots of mean tracer concentration obtained from the LB simulations, at various times, as a function of distance from the inlet of the channel were compared with the analytical solutions. Figure 7 summarizes the comparison between the LB results for $\tau = 0.7$ and the analytical solutions from the Taylor–Aris theory using Equation (33).

The LB simulation carried out on a 41×1000 lattice for $\tau = 0.7$ and $V_{x_{\max}} = 0.1$ can be related to a typical tracer dispersion problem with realistic physical parameters.

Example

A step input of the tracer is imposed at the inlet of a capillary of size 1 mm diameter through which water is moving with an average velocity of 1.2638 m day^{-1} (a typical pore velocity,

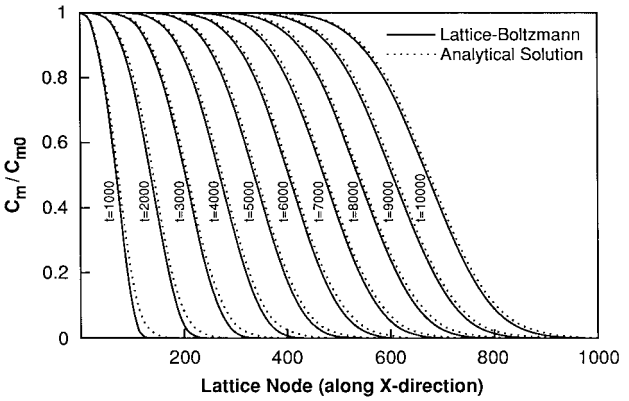

Figure 7. Comparison between the LB results for dispersion in a channel at $\tau_s = 0.7$ and the analytical solutions from the Taylor–Aris theory using Equation (33).

assuming a parabolic velocity profile). The tracer has a diffusivity of 2.35×10^{-9} m^2 s^{-1}. Calculate the actual physical time which corresponds to the concentration profile of the tracer obtained after 10000 lattice times in the LB method.

Solution

The Peclet number is given by

$$Pe = \frac{Uh}{D}, \tag{35}$$

where U is the average velocity $= (2/3)U_{\max}$; h is the channel width and D is the dispersion coefficient. Using Equation (31),

$$D_{\mathrm{LB}} = 0.5007 \tag{36}$$

and

$$Pe_{\mathrm{LB}} = \frac{0.06666 \times 41}{0.5007} = 5.458. \tag{37}$$

$$D_{(\text{real problem})} = 2.68 \times 10^{-9} \tag{38}$$

and

$$Pe_{(\text{real problem})} = 5.458. \tag{39}$$

Since the Peclet numbers are the same in both cases, the dimensionless times can be compared.

$$t' = \frac{t}{(h/U)}. \tag{40}$$

Using $t'_{(\mathrm{LB})} = t'_{(\text{real problem})}$, it is found that $t = 21.128$ min.

Figure 7 plots the concentration as a function of distance along the channel (measured in lattice units). With reference to the problem considered above, each lattice unit in Figure 7 corresponds to 1/41 mm.

4.3. Results of dispersion in the expansion–contraction geometry

The dispersion simulations were also carried out for a 241×1000 lattice for the expansion–contraction geometry. Results are presented for $\tau = 0.7$ and $\tau = 10.0$. For the study of dispersion, steady state flow was first achieved as mentioned earlier. At steady state, a step input of tracer was introduced at the inlet ($x = 1$) according to Equation 34, and the cup-mixed mean concentration was monitored at the cross-section, where $x = 650$ (downstream of the contraction). Figure 8(a) and (b) plot the cup-mixed mean concentration as a function of time for $\tau = 0.7$ and $\tau = 10$ respectively.

A plot of dimensionless point concentration of the tracer at $x = 520$ (halfway through the dilation) at time $t = 50000$ is shown in Figure 9(a) and (b) for $\tau = 0.7$ and $\tau = 10$ respectively, and is compared with results from FIDAP. As can be seen from the comparison of the cup-mixed mean concentration and the point concentration at $\tau = 0.7$, there is excellent agreement between the LB method and FIDAP. For $\tau = 10.0$, the agreement is not so good.

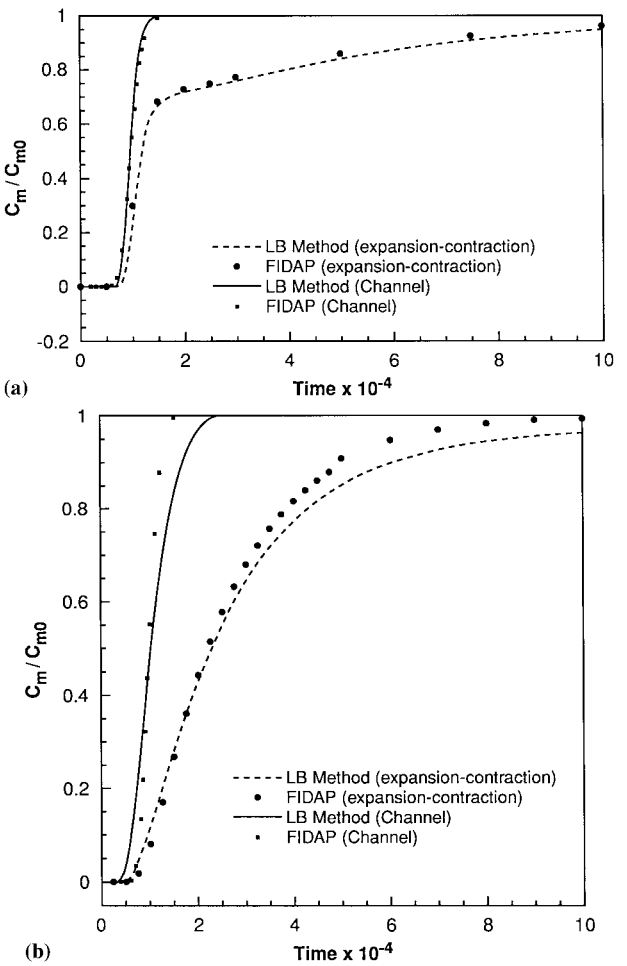

Figure 8. Dispersion in the expansion–contraction geometry. Plots of mean concentration at $x = 650$ as a function of time for (a) $\tau = 0.7$ and (b) $\tau = 10$.

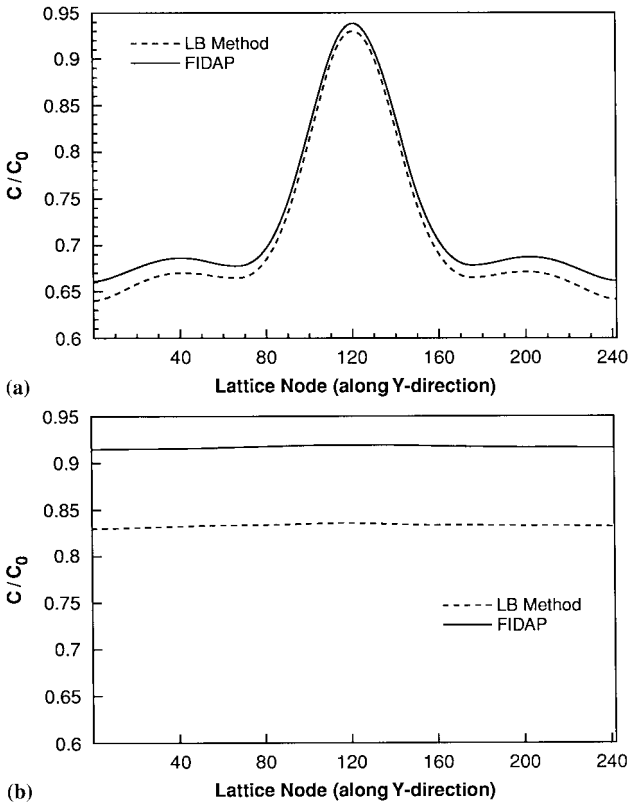

Figure 9. Plot of dimensionless point tracer concentration at $x = 520$ (half way through the dilation) at time $t = 50000$ for (a) $\tau = 0.7$ and (b) $\tau = 10$.

4.4. Error analysis for dispersion

The effect of the value of τ and lattice refinement has been studied in the case of Taylor–Aris dispersion. For the solvent, a parabolic velocity profile was imposed at all cross-sections of the channel with a maximum velocity of 0.1 at the center, for 11×1000, 21×1000 and 41×1000 lattice. When the steady state for the solvent was achieved, a step input of the tracer was introduced at the inlet of the channel. The mean tracer concentration obtained from the LB simulations, at 5000 lattice time units at a distance from the inlet of the channel were compared with the analytical solutions. The quantity $c_{\mathrm{m(LB)}}/c_{\mathrm{m(Theoretical)}}$ at the point where mean concentration should be $0.5C_{\mathrm{m0}}$ (based on the analytical solution) has been plotted as a function of τ/h, which is proportional to the Knudson number. It may be seen from Figure 10 that the error in the mean concentration is minimal until $\tau/h < 0.08$ (for the range of τ between 0.7 and 10.0). It was also observed that for a given lattice, error in the tracer calculations reaches a minimum at $\tau = 1.0$.

5. LEAKY WALLS IN THE LB METHOD

Leaks in the population of LB fluid particles are natural to the LB method, especially in the case of the energy boundary conditions. At each time step, LB particles leave and enter from

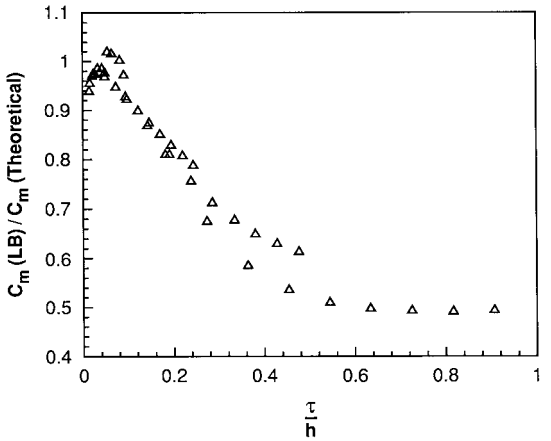

Figure 10. C_m(LB)/C_m(theoretical) at the point where mean concentration should be (based on the analytical solution) $0.5C_{m0}$ has been plotted as a function of τ/h using results obtained by 11×1000, 21×1000 and 41×1000 lattices.

the boundaries. A mismatch between the incoming and outgoing masses (no matter how small), leads to a diminution/addition of the mass of LB fluid particles, causing so-called 'leaky' walls. However, the presence of leaky walls does not mean that the actual fluid being simulated is leaking from the walls. The kinematic viscosity of the LB fluid is independent of density (depends on value of the τ) indicating that a change in density at a point will cause a change in viscosity of the LB fluid particles at that point, hence, the Reynolds number being simulated will not be effected.

It was also observed that leaks are a direct consequence of the compressibility of the LB fluid. The leak of the LB particles approaches zero as the Mach number approaches zero. Figure 11 shows the results of the two simulations carried out for channel flow. In the first case, the center velocity of the parabolic profile imposed at the inlet and outlet of the channel was 0.1 ($V_{x_{avg}} = 0.0666$), and in the second case, the velocity at the center was 0.05 ($V_{x_{avg}} = 0.0333$). It may be seen from the Figure 11 that when the velocity at the center was 0. 1, an initial system mass of 21000 becomes about 25000 at steady state, whereas in the second case, when the velocity at the center is 0.05, the system mass at the steady state becomes about 22000. In general, system mass may increase or decrease as a function of time, depending on

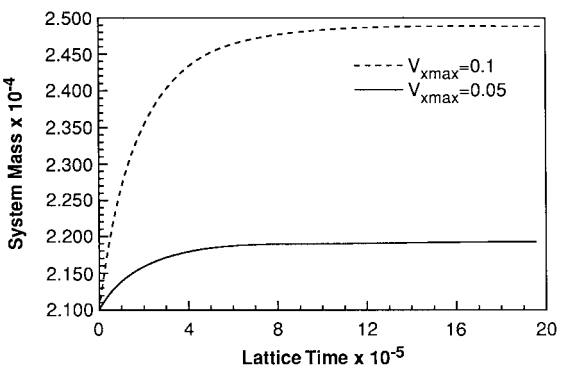

Figure 11. System mass as a function of the lattice time in case of the channel flow.

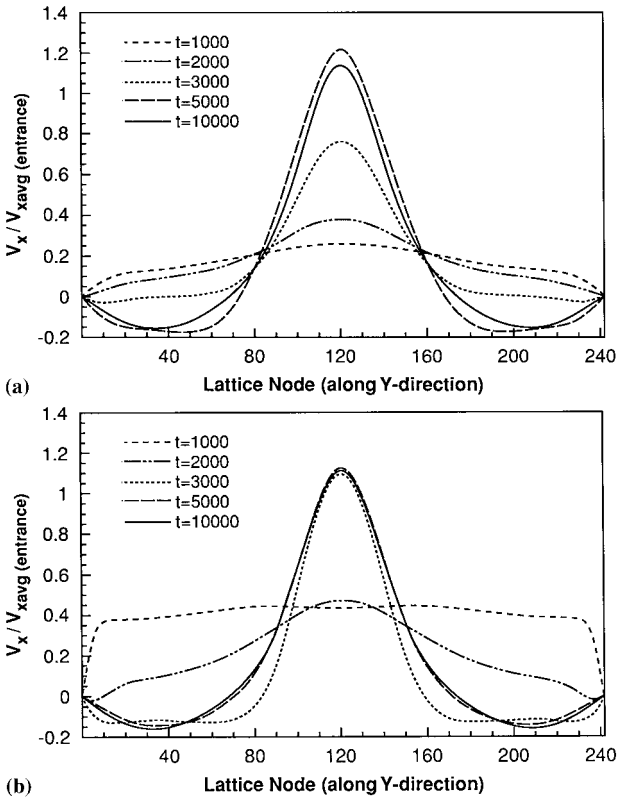

Figure 12. The x component of the velocity at $x = 520$ along the y-direction as a function of time using (a) FIDAP and (b) the LB method.

geometry, τ and velocity. In all the cases, leaking decreases as the steady state solution is approached. This criterion may be used to check whether the steady state is reached or not.

6. TRANSIENT SOLUTION

A comparison between the LB method and FIDAP was carried out for the analysis of transients in the expansion–contraction geometry. Figure 12(a) and (b) plots the x component of the velocity at $x = 520$ as a function of lattice time. It is natural to have the discrepancy between the LB method and FIDAP in the initial time interval because whereas the speed of sound in the LB method is finite, it is infinite when we solve the incompressible Navier–Stokes equation using FIDAP. As a result, while a disturbance in the fluid takes a finite amount of time to move from one point to another in the LB method, it is felt immediately throughout the flow domain in the incompressible FIDAP solution. However, once the effect of the disturbance has propagated in the flow domain, the results of the LB method and FIDAP come closer and closer.

7. PRESSURE-DRIVEN FLOW

Pressure driven flow can be solved using the LB method using energy boundary conditions. The pressure gradient can be set between the inlet and outlet ends of the pipe by imposing a density gradient, since the density is proportion to the pressure. The incoming values of the $f_{\sigma i}$ can be calculated using Equations (16)–(20). Results for pressure-driven Poiseuille flow are shown in Figure 13(a) and (b). The pressure drop in this simulation was achieved by imposing a density difference between the inlet and outlet ($\rho = 1.0$ at the inlet and $\rho = 0.95$ at the outlet). Energy boundary conditions were then applied at the inlet, the outlet and the walls to calculate the unknown $f_{\sigma i}$. The density gradient along the length of the pipe at steady state is shown in Figure 13(b). There was no variation in density across the channel. A comparison of the velocity profile calculated from the LB method with the analytical result is shown in Figure 13(a). Excellent agreement is seen between theory and the LB simulation indicating the utility of the energy boundary condition in solving pressure-driven flows.

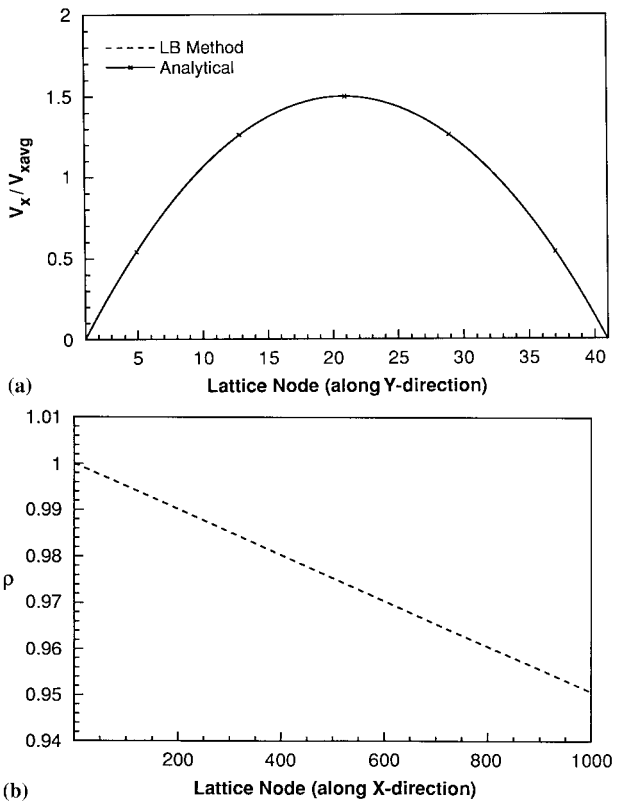

Figure 13. (a) Velocity profiles for pressure-driven flow between two parallel plates. (b) Density profile along the channel.

8. SUMMARY

We have successfully demonstrated the application of the LB method to two problems related to the study of flow and dispersion in a porous media: Poiseuille flow and flow in an expansion–contraction geometry. Bounce back and energy boundary conditions were tested for the flow problem in the expansion–contraction geometry and an excellent agreement was found with results obtained using FIDAP. For dispersion, τ values in the range 0.7–10 were investigated. It was found that the error in the dispersion results become minimum at $\tau = 1$.

Results for transient flow in an expansion–contraction geometry obtained using the LB method and FIDAP were also compared, and it was found that at the short times, LB results do not quite agree with the results obtained using FIDAP. The disagreement was attributed to the finite velocity of sound implicit in the LB method. Another problem of interest, pressure-driven flow was investigated, and the utility of the energy boundary condition was demonstrated.

The LB technique is easily implemented on parallel architecture. Complex boundaries are also easily implemented, which makes it suitable for the study of flow in porous media.

ACKNOWLEDGMENTS

This work was sponsored in part by the Army High Performance Computing Research Center under the auspices of the Department of Army, Army Research Laboratory cooperative agreement number DAAH04-95-20003/contract # DAAH04-95-C-0008, the content of which does not necessarily reflect the position or policy of the government and no official endorsement should be inferred. Computational resources were partly provided by the Minnesota Supercomputer Institute (MSI). D.M.K. acknowledges support from the National Science Foundation under Grant No. DMR-9405824 and donors of the Petroleum Research Fund, administered by the ACS.

APPENDIX A. NOMENCLATURE

c_s	velocity of sound
C	point concentration of the tracer
C_0	concentration of the tracer at the inlet
C_m	mean concentration of the tracer
C'_m	dimensionless mean concentration of the tracer
C_{m0}	inlet mean concentration of the tracer
ΔC_m	difference in mean concentration
d	diameter of the pipe
D	dispersion coefficient of the tracer
D_m	molecular diffusivity of the tracer
$\mathbf{e}_{00}$	null velocity vector
$\mathbf{e}_{1i}$, $\mathbf{e}_{2i}$, $i = 1$–4	velocity unit vector directions
f	distribution function for the main fluid
$f_{\sigma i}$	particle distribution function for component σ and velocity direction i
$f_{\sigma i(s)}$	tracer distribution function

$f^{eq}_{\sigma i}$	equilibrium particle distribution function for component σ and velocity direction i
$f^{eq}_{\sigma i(s)}$	equilibrium particle distribution function for component σ and direction i for the tracer
h	height of the channel
n_s	tracer concentration (LB)
n_0	desnsity of the main fluid (LB)
p	pressure
Pe	Peclet number
r	radius of the pipe
R_s	reaction rate
t	time
t'	dimensionless time
$\mathbf{u}$	velocity vector
U	mean velocity of the fluid
V_x	x component of the velocity
V_y	y component of the velocity
$V_{x_{avg}}$	average x component of the velocity
$V_{x_{max}}$	maximum x component of the velocity
x	x distance
x'	dimensionless x distance

Greek letters

ε	lattice Boltzmann internal energy
δ	Knudsen number
v	kinematic viscosity
ρ	density of pseudo-fluid particles
τ	relaxation time for the main fluid
τ_s	relaxation time for tracer
$\Omega_{\sigma i}$	collision operator

REFERENCES

1. G. McNamara and G. Zanetti, 'Use of the Boltzmann equation to simulate lattice gas automata', *Phys. Rev. Lett.*, **61**, 2332–2335 (1988).
2. F. Higuera and J. Jimenez, 'Lattice gas dynamics with enhanced collision', *Europhys. Lett.*, **9**, 663–668 (1989).
3. H. Chen, S. Chen and W.H. Matthaeus, 'Recovery of the Navier–Stokes equation using a lattice Boltzmann method', *Phys. Rev. A*, **45**, R5339–R5342 (1991).
4. Y.H. Qian, D. d'Humieres and P. Lallemand, 'Lattice BGK models for the Navier–Stokes equation', *Europhys. Lett.*, **17**, 479–484 (1992).
5. S.Y. Chen, H.D. Chen, D. Martinez and W.H. Matthaeus, 'Lattice-Boltzmann model for simulation of magnetohydrodynamics', *Phys. Rev. Lett.*, **67**, 3776–3779 (1991).
6. P. Bhatnagar, E.P. Gross and M.K. Krook, 'A model for collision processes in gases. I. Small amplitude processes in charged and neutral one component systems', *Phys. Rev.*, **94**, 511–525 (1954).
7. A.K. Gunstensen, D.H. Rothman and S. Zaleski, 'Lattice-Boltzmann model of immiscible fluids', *Phys. Rev. A*, **43**, 4320 (1991).
8. D. Grunau, S. Chen and K. Eggert, 'A lattice-Boltzmann model for multiphase fluid flows', *Phys. Fluids A*, **5**, 2557 (1993).
9. D. Martinez, S. Chen and W.H. Mattaeus, 'Lattice-Boltzmann magnetohydrodynamics', *Phys. Plasma*, **1**, 1850 (1994).
10. S.P. Dawson, S. Chen and G. Doolen, 'Lattice-Boltzmann computations for reaction–diffusion equations', *J. Chem. Phys.*, **98**, 1514 (1993).

11. S. Hou, 'Lattice-Boltzmann method for incompressible, viscous flow', *Ph.D. Dissertation*, Kansas State University, Manhattan, KS, 1995.
12. D.W. Ruth and H. Ma, 'Numerical analysis of viscous, incompressible flow in a diverging–converging RTU', *Trans. Porous Media*, **13**, 161 (1993).
13. D.R. Noble, J.G. Georgiadis and R.O. Buckius, 'Comparison of accuracy and performance for lattice-Boltzmann and finite difference simulations of steady viscous flow', *Int. J. Numer. Methods Fluids*, **23**, 1–18 (1996).
14. H. Brenner and D.A. Edwards, *Macrotransport Processes*, Butterworth-Heinemann, Boston, 1993.
15. D. d'Humieres and P. Lallemand, 'Numerical simulations of hydrodynamics with lattice gas automata in two dimensions', *Complex Syst.*, **1**, 599 (1987).
16. R. Cornubert, D. d'Humieres and D. Levermore, 'A Knudsen layer theory for lattice gases', *Physica D*, **47**, 241 (1991).
17. I. Ginzbourg and P.M. Adler, 'Boundary flow condition analysis for the three-dimensional lattice-Boltzmann model', *J. Phys. II France*, **4**, 191 (1994).
18. P.A. Skordos, 'Initial and boundary conditions for the lattice-Boltzmann methods', *Phys. Rev. E*, **48**, 4823–4842 (1993).
19. D.R. Noble, S. Chen, J.G. Georgiadis and R.O. Buckius, 'A consistent hydrodynamic boundary condition for the lattice-Boltzmann method', *Phys. Fluids*, **7**, 203–209 (1995).
20. D.R. Noble, J.G. Georgiadis and R.O. Buckius, 'Direct assessment of lattice-Boltzmann hydrodynamics and boundary conditions for recirculating flows', *J. Stat. Phys.*, **81**, 17–33 (1995).
21. G.I. Taylor, 'Dispersion of soluble matter in solvent flowing slowly through a tube', *Proc. R. Soc. A*, **219**, 186 (1953).
22. R. Aris, 'On the dispersion of a solute in a fluid flowing through a tube', *Proc. R. Soc. A*, **235**, 67 (1956).

